



Published in final edited form as:

Am J Clin Pathol. 2014 May ; 141(5): 639–647. doi:10.1309/AJCPVWH1K2ZIHHTV.

BRAF Pyrosequencing Analysis Aided by a Lookup Table

Matthew T. Olson, MD¹, Colleen Harrington¹, Katie Beierl, MS¹, Guoli Chen, MD¹, Michele Thiess¹, Alan O'Neill¹, Janis M. Taube, MD², Martha A. Zeiger, MD³, Ming-Tseh Lin, MD¹, and James R. Eshleman, MD^{1,4}

¹Department of Pathology, The Johns Hopkins University School of Medicine, Baltimore, MD

²Department of Dermatology, The Johns Hopkins University School of Medicine, Baltimore, MD

³Department of Surgery, The Johns Hopkins University School of Medicine, Baltimore, MD

⁴Department of Oncology, The Johns Hopkins University School of Medicine, Baltimore, MD

Abstract

Objectives—*BRAF* mutations have substantial therapeutic, diagnostic, and prognostic significance, so detecting and specifying them is an important part of the workload of molecular pathology laboratories. Pyrosequencing assays are well suited for this analysis but can produce complex results. Therefore, we introduce a pyrosequencing lookup table based on Pyromaker that assists the user in generating hypotheses for solving complex pyrosequencing results.

Methods—The lookup table contains all known mutations in the sequenced region and the positions in the dispensation sequence at which changes would occur with those mutations. We demonstrate the lookup table using a homebrew dispensation sequence for *BRAF* codons 596 to 605 as well as a commercially available kit-based dispensation sequence for codons 599 to 600.

Results—These results demonstrate that the homebrew dispensation sequence unambiguously identifies all known *BRAF* mutations in this region, whereas the kit-based dispensation sequence has one unresolvable degeneracy that could be solved with the addition of two injections.

Conclusions—Using the lookup table and confirmatory virtual pyrogram, we unambiguously solved clinical pyrograms of the complex mutations V600K (c.1798_1799delGTinsAA), V600R (c.1798_1799delGTinsAG), V600D (c.1799_1800delTGinsAT), V600E (c.1799_1800delTGinsAA), and V600_K601delinsE (c.1799_1801delTGA). In addition, we used the approach to hypothesize and confirm a new mutation in human melanoma, V600_K601delinsEI (c.1799_1802delTGAAinsAAAT).

Keywords

BRAF mutations; Pyrosequencing; Pyromaker; Pyrosequencing analysis; Bioinformatics

The proto-oncogene *BRAF* (v-Raf murine sarcoma viral gene homolog B1) is a well-known component of the MEK/MAPK pathway that plays a critical role in cell growth. This

component was first demonstrated elegantly and comprehensively by Davies et al¹ in 2002. Mutations in *BRAF* have been identified in numerous malignant neoplasms including melanoma, papillary thyroid carcinoma, colorectal carcinoma, non-small cell lung cancer, and hairy cell leukemia.¹⁻⁵ Moreover, these mutations are increasingly recognized for their diagnostic, prognostic, and therapeutic implications. A *BRAF* V600E (c.1799T>A) mutation has a positive predictive value for papillary thyroid carcinoma that may approach 100%^{6,7} and likely is associated with local recurrence and poor clinical outcomes.^{8,9} Mutated *BRAF* blunts the response to anti-epidermal growth factor receptor therapy in patients with metastatic colorectal adenocarcinoma.¹⁰ Furthermore, *BRAF* mutations may be targetable; the *BRAF* inhibitor vemurafenib was recently approved by the Food and Drug Administration (FDA) for unresectable or metastatic melanoma. Its indications are limited to tumors harboring the activating *BRAF* V600E (c.1799T>A) mutation. A new drug application for a second drug, dabrafenib, has also been submitted for the treatment of V600E-bearing melanoma.

Given the significance of *BRAF* mutations in diagnosis and clinical management, the reporting of *BRAF* mutational status of papillary thyroid carcinoma, lung and colorectal adenocarcinoma, and malignant melanoma has become routine pathology practice. Although V600E (c.1799T>A) represents approximately 95.9% of all *BRAF* mutations, other mutations are occasionally encountered. For example, V600E (c.1799_1800delTGinsAA) accounts for approximately 74% of non-V600E (c.1799T>A) *BRAF* mutations in malignant melanoma, whereas V600K (c.1798_1799delGTinsAA) represents 20%, and other mutations comprise approximately 6%.¹¹ Moreover, different *BRAF* mutations appear to be associated with unique clinicopathologic features.^{12,13} Thus, an ideal *BRAF* assay should be able to detect non-V600E (c.1799T>A) mutations, and these specific *BRAF* base changes should be reported rather than merely stating the presence or absence of a *BRAF* mutation.

Pyrosequencing is commonly used to detect *BRAF* mutations.¹⁴ Compared with Sanger sequencing, pyrosequencing is inherently more quantitative, has a superior limit of detection (5% minor allele frequency), and is faster.¹⁵⁻¹⁷ However, pyrograms of complex mutations can generate confusing patterns that are often difficult to resolve without further investigation. To assist in the resolution of complex pyrograms, we recently developed a freely available software program, Pyromaker (<http://pyromaker.pathology.jhmi.edu>), which generates simulated traces for pyrosequencing results based on user inputs.¹⁸ Although Pyromaker is useful in the iterative hypothesis testing of solutions for complex pyrosequencing results, our first validation¹⁸ dealt primarily with complex *KRAS* mutations with pyrograms that involved three or four peak differences. By contrast, complex *BRAF* mutations commonly produce pyrograms with more than twice that number of peak differences, so even the process of hypothesis generation can be challenging.

In this study, we introduce the use of Pyromaker to make a lookup table for all known mutations of the sequenced region detected with a dispensation sequence. We show that the use of a lookup table followed by a confirmatory virtual trace comparison leads to rapid and unambiguous identification of all known *BRAF* mutations in the region of interest. Furthermore, we show that the lookup table facilitates a critical evaluation and rational choice of the dispensation sequence used in mutational analysis.

Materials and Methods

Pyromaker

The general features and specifications of Pyromaker have been previously described.¹⁸ The application of Pyro-maker in the current study differed in two ways from the previous publication. First, peak magnitudes of the pyrogram were exported to obtain the positions in the pyrogram for which the mutant sequence differed from the wild-type sequence. Second, annotations of these differences were added automatically to the virtual pyrogram. These features were made available in an update to the freely available public version (<http://pyromaker.pathology.jhmi.edu>). Using these modifications, Pyromaker generated a list of altered peaks for all of the relevant mutations recorded in the Catalogue of Somatic Mutations in Cancer (COSMIC) at the Sanger Institute (Cambridge, England; <http://www.sanger.ac.uk/genetics/CGP/cosmic>, last accessed November 12, 2012) and all hypothetical single-point mutations for codon 600. All virtual pyrograms were plotted assuming a heterozygous mutant allele and a 100% tumor cellularity so that the signal from the mutant DNA comprised 50% of the total signal. For comparison with the clinical pyrograms, the homebrew dispensation sequence, which was developed for mutations from *BRAF* codons 596 to 605, was GTAGCTAGCTAT-CAGCATCGACTCTCGATGAGTG, where the nucleotide triphosphates are simply listed as single characters in the preceding sequence. For the analysis of the kit-based dispensation sequence available from Qiagen (Valencia, CA), the reverse dispensation sequence TCGTATCTGTAG was used. In virtual pyrograms, as in actual pyrograms, a position refers to one deoxyribonucleotide triphosphate (dNTP) injection (“dispensation”) on the x axis.

Sample Preparation and DNA Extraction

BRAF mutations were detected in the clinical molecular laboratory during routine analysis. The V600_K601delinsE (c.1799_1801delTGA) was found in primary papillary thyroid carcinoma, and the classic V600E (c.1799T>A) was found in primary malignant melanoma. All other mutations were found in specimens with metastatic melanoma. After H&E-stained slide review and tumor tissue selection, the corresponding tissue from five unstained, 5- μ m-thick tissue sections was manually microdissected using Pinpoint reagents according to the manufacturer's protocol (ZymoResearch, Orange, CA). DNA was purified from the sample using the QIAmp DNA kit (Qiagen) and quantified by OD 260 nm. To ensure the appropriate sensitivity of the homebrew dispensation sequence, the peak height of the mutant peak corresponding to c.1799T>A was measured with the methods involving the kit-based and homebrew dispensation sequences. The *BRAF* mutation status of the *BRAF*-mutated RKO cell line was tested with each method undiluted and at dilutions of 1:1, 1:2, 1:5, 1:10, 1:20, and 1:100 to *BRAF* wild-type DNA. This validation is shown in Supplemental Table 1. (All supplementary materials can be viewed at http://s3.amazonaws.com/ascpcdn/static/ASCPResources/Press/AJCP/May2014_Olsonpdf)

Pyrosequencing

Samples were amplified using polymerase chain reaction (PCR) in a 25- μ L reaction containing 0.2 μ mol/L forward primer (5'-GAAGACCTCACAGTAAAATAG-3'), 0.2 μ mol/L reverse primer (5'-biotin~ATAGCCTCAATTC-TTACCATCC-3'), 0.16 μ L

HotStarTaq DNA polymerase (Qiagen), 0.15 mmol/L magnesium chloride (Qiagen), 0.15 mmol/L dNTPs (Applied Biosystems, Foster City, CA), and 2.5 μ L PCR buffer (Qiagen). Samples were amplified in a Veriti thermal cycler (Applied Biosystems) with the following conditions: 95°C for 15 minutes, 42 cycles (95°C for 20 seconds, 53°C for 30 seconds, and 72°C for 20 seconds), and 72°C for 5 minutes. The amplicons were sequenced using PyroMark Gold reagents (Qiagen) on a PyroMark Q24 instrument (Qiagen). The sequencing reagents contained 0.3 μ mol/L sequencing primer (5'-GACCTCACAG-TAAAAATAGGTGATTTTG-3') and annealing buffer. The nucleotide dispensation order used for codons 596 to 606 was GTAGCTAGCTATCAGCATCGACTCTCGATGAGTG.

Sanger Sequencing

Samples were PCR amplified using the same conditions as those used for pyrosequencing but using M13-tailed primers with the following sequences: 5'-M13F-TTCTTCAT-GAAGACCTCACAG-3' (forward) and 5'-M13R-GTG-GAAAAATAGCCTCAATTCTTAC-3' (reverse). Amplicons were purified using ExoStar (GE Healthcare, Piscataway, NJ) and sequenced using BigDye v3.1 reagents (Applied Biosystems). Sequencing products were purified with BigDye XTerminator reagents (Applied Biosystems), and bidirectional sequencing was performed on an ABI 3500xl (Applied Biosystems) capillary electrophoresis instrument.

Results

All Known *BRAF* Mutations Produce Distinct Pyrograms With the Homebrew Dispensation Sequence

We identified all known mutations in the *BRAF* oncogene in COSMIC and produced the expected pyrosequencing traces using Pyromaker, inputting either our homebrew dispensation sequence or the dispensation suggested in the Qiagen *BRAF* pyrosequencing kit. The homebrew dispensation has the advantages that (1) the sequence is the forward sequence, (2) the 1 \times peak height is well defined before sequencing through the V600 region, and (3) it can detect rare mutations down- and upstream from the V600 codon. We then tabulated all the peaks that were at new positions or at existing positions where the peak was either increased or decreased. The expected peak changes for all known *BRAF* mutations gave distinct patterns with the homebrew dispensation sequence. Table 1 lists all the activating *BRAF* mutations and the mutations discussed here¹⁹⁻²⁵; the complete list is shown in Supplemental Table 2. As seen in this Table, some mutations do not result in novel peaks and are only manifest as changes in the height of wild-type peaks. These are considerably more difficult to detect. This occurs in another gene, *KRAS* with the G12V mutation, that results from a GGT>GTT mutation that is manifest only as a reduction of G activity and increase in T activity. With *BRAF*, these are only seen in the relatively rare mutations c.A1791G, c.G1792A, and c.C1793T shown in Supplemental Figure 1A, Supplemental Figure 1B, and Supplemental Figure 1C, respectively.

Virtual pyrograms for each of the mutations listed in Table 1 are shown in Supplemental Figure 1, Supplemental Figure 2, and Supplemental Figure 3. Peak-change combinations alone were inadequate to resolve all mutations. Two combinations, the change of positions 7

and 8 Supplemental Figure 4A and the change of positions 20 and 21, had ambiguities that required information about whether the peak magnitude had increased or decreased Supplemental Figure 4B to definitively define them. For example, the L597L (c.1791A>G) mutation leads to a decrease in signal at the seventh position (A) and an equivalent increase in the eighth position (G), whereas the A598T (c.1792G>A) mutation produces opposite changes Supplemental Figure 4D. The change in direction was useful in the more complex combination of peaks produced by both V600_S605delinsD (c.1799_1814delinsA) and V600_S605delinsEK (c.1799_1815delinsAAAAG) Supplemental Figure 4C and Supplemental Figure 4F. In this case, the direction of change in the 20th position—decreased for V600_S605delinsD (c.1799_1814delinsA) and increased for V600_S605delinsEK (c.1799_1815delinsAAAAG)—led to the correct distinction between these two pyrograms.

Use of the Kit Dispensation Sequence

Applying the kit-based dispensation sequence, the expected peak changes for all known *BRAF* mutations in the sequencing region of the homebrew dispensation sequence are shown in Table 1. The reverse (antisense) sequence was used for the analysis because that is the sequencing direction used by the kit-based approach. All three degenerate sets have peak changes in exactly the same directions. Two of the three degenerate pyrograms show peak changes that were resolved unambiguously with peak ratios. The ratio of change in the second and fourth positions was 0.5 for the V600R (c.1798_1799delGTinsAG) mutation and 2.0 for the V600G (c.1799T>G) mutation Supplemental Figure 5A and Supplemental Figure 5E. Similarly, the ratio of change in the fourth and fifth positions was 1.0 for the insertion of TAC after codon 599 and 2.0 for the V600K (c.1798_1799delGTinsAA) mutation Supplemental Figure 5B and Supplemental Figure 5F. One degenerate set could not be resolved using the kit-based dispensation sequence; the A598V (c.1793C>T) and A598_T599insV (c.1794_1795insGTT) mutations produced identical pyrograms because the insertion of GTT disrupted the final positions in the kit dispensation sequence Supplemental Figure 5C and Supplemental Figure 5G. Virtual pyrograms showed that extending the kit-based dispensation sequence by C and G or C and T injections would resolve this degeneracy as the polymerase would advance first to the C in either case and then to a G in the case of the insertion or to a T in the case of the substitution Supplemental Figure 5D vs Supplemental Figure 5H.

Resolving Simple and Complex *BRAF* Pyrograms With a Lookup Table

Applying the findings of Table 1 to the clinical pyrograms seen in Figure 1, usual and unusual *BRAF* mutations were identified unambiguously with the pyrosequencing results alone. In cases A and B, the single and double substitution had only two peak changes, which were identified with minimal effort. Cases C and D had seven and eight peak changes, respectively. The affected peak positions were unique to those two mutations. As such, they were identified as V600K (c.1798_1799delGTinsAA) and V600R (c.1798_1799delGTinsAG) with the same lookup operation used in the simpler cases. The mutations were confirmed with a virtual pyrogram that matched the clinical pyrograms exactly. The unusual *BRAF* mutant sequences were additionally confirmed with Sanger sequencing Figure 2B, Figure 2C, and Figure 2D.

Resolving V600E (c.1798_1799delGTinsAA) and V600_K601delinsE (c.1799_1801delTGA)

The clinical pyrograms shown in Figure 3A and Figure 3B involve the same peaks, all of which were changed from the wild-type pyrogram in the same direction. Using the lookup table from Table 1, it was evident that the mutations were clearly either V600E (c.1799_1800delTGinsAA) or V600_K601delinsE (c.1799_1801delTGA). This ambiguity was resolved with Pyromaker-generated plots of the virtual pyrograms, shown below the clinical pyrograms in Figure 3. As seen in the virtual pyrograms, the first two altered peaks—in positions 17 and 19—were altered at different ratios. In the case of V600E (c.1799_1800delTGinsAA), these peaks occurred with a ratio of 5.5, whereas in V600_K601delinsE (c.1799_1801delTGA), the same peaks occurred with a ratio of 2.2. Because both peaks are caused by sequencing of the mutant and not the wild-type DNA, the ratio between them was independent of zygosity and tumor-cell composition. The V600E (c.1799_1800delTGinsAA) mutation was confirmed using Sanger sequencing and shown in Figure 2E.

Hypothesis-Based Pattern Matching of a New Mutation

The lookup table in Table 1 failed to identify the mutation in the clinical pyrogram Figure 4A; there was no mutation with changes at positions 17, 20, and 21 because this mutation is novel and not previously reported in COSMIC. A lookup table of combinations of mutations was made. The mutations that were combined were chosen because they involved positions 17, 20, and 21. The table can be found in Supplemental Table 3. The only solution that matched this peak-change combination was V600_K601delinsEI (c.1799_1802delTGAAinsAAAT). The V600E (c.1799_1800delTGinsAA) and K601I (c.1802A>T) were determined to be on the same strand of mutant DNA because a combination of two mutant populations could not cause the marked increase in the A peak at position 17 even if the maximum amount of tumor harbored the V600E (c.1799_1800delTGinsAA) mutation (data not shown). The V600_K601delinsEI (c.1799_1802delTGAAinsAAAT) mutation was confirmed with Sanger sequencing and shown in Figure 2F.

Discussion

The Virtual Pyrogram Lookup Table

Simple lookup tables such as the one described herein are suitable for problems involving small searches of limited data sets when the search and the result are exact matches. The searches presented herein are short because the clinical pyrogram is interpreted as a list of dispensation positions with changes from the wild-type pyrogram. The lookup table is also small because the sequenced *BRAF* gene and almost all mutations are known or are combinations from known mutations. Lookup tables have also been used on larger scales to simplify traditionally computationally intensive calculations²⁶ and in peptide sequencing.²⁷ When nonexact matching is introduced, the applications become even more abundant and have been widely used in the analytical chemistry laboratory to identify small molecules based on fragmentation patterns²⁸ and to accurately characterize protein classes in tissues.^{29,30} Genetic data analysis frequently involves matching small searches against very large data sets, so the problem space becomes so large that matching to a table is inefficient. Lookups in those settings are implemented as exact matching in sophisticated suffix trees,

such as those used in efficient linear matching.³¹ Although more elaborate algorithms have applications in larger problems in molecular genetics, the interpretation of the clinical pyrogram is limited to specific genes and interpretation by a molecular pathologist. Thus, the approach presented herein is the ideal match of sophistication for practical molecular pathology workflows.

Necessity of the Virtual Pyrogram Lookup Table

We previously demonstrated the use of virtual pyrograms as a useful tool in iterative problem solving when complex pyrosequencing is difficult to interpret.¹⁸ Our previous study focused primarily with *KRAS* mutations in codons 12 and 13, and the most complex result involved peak changes at only four dispensation positions. As such, a human could iterate through hypothetical solutions to the correct mutation with little effort, and the starting solutions were chosen easily based on the small number of changed pyrogram peaks. By contrast, the results presented here demonstrate multiple peak changes. Although the previously described pathologist-guided approach to solving pyrograms is still valid, a de novo starting point for numerous peak changes requires significant effort. To address this issue, we now present a novel pyro-sequencing analysis approach that uses a lookup table to expedite the first—and usually the correct—hypothesis. For currently known *BRAF* mutations, the pyrosequencing results resolve the mutations unambiguously. However, exhaustive testing of every imaginable mutation is not computationally feasible in the clinical setting, so there remains a possibility that unusual pyrograms may match the lookup table yet represent either a degenerate solution or a new mutation that is degenerate with one already described. Thus, the lookup table solution must be followed with a confirmatory virtual pyro-gram comparison to ensure that the solution yields the correct peak proportions and directions.

Scalability of the Virtual Pyrogram Lookup Table

Although the results are centered on *BRAF* pyrogram interpretation, the same approach could be applied to any clinical pyrosequencing assay. In fact, generating a lookup table for expected mutations is most desirable in the validation stage of assay development because dissimilar mutations can produce similar pyrograms. In the development of a rugged assay, increased resolution can often be gained by adding different stations in the dispensation sequence or by confirming that changes in the direction or ratio between peaks in degenerate pyrograms occur in a reproducible and dependable manner.

If an assay is robust to detect mutations in a well-characterized gene, it is plausible to envision automating the lookup table approach for in silico assignment of the mutation status, and this is ultimately the goal for increasingly multiplexed molecular assays. However, such an approach will involve several technical and regulatory complications. These complications include the need to normalize the pyrogram signal; standardize the representation of the pyrogram for automated pattern matching; validate the process and institute proficiency testing of automated pattern matching for molecular results, especially to account for low-signal mutations; and institute commensurate billing and reimbursement changes. Although the approach presented here is a necessary advancement toward automated analysis, it is not currently sufficient to use this approach in this way.

Superiority of the Homebrew Dispensation Sequence

The results presented herein demonstrate how the homebrew dispensation sequence enables the unambiguous identification of all known *BRAF* mutations from codon 596 to 605, whereas the less exhaustive kit-based dispensation sequence is shown to miss all mutations upstream to codon 598 and gives an unresolvable result for two mutations at codon 598. In addition, because the 1801 nucleotide is upstream from the sequencing region of the kit-based assay, it may not sequence the V600_K601delinsE (c.1799_1801delTGA) mutation. This is a known activating mutation, so failure to recognize it could lead to underuse of the targeted *BRAF* inhibitor therapy. The significance of this particular mutation should be evaluated in each specific laboratory; the key finding is that the lookup table method presented herein predicts assay performance and enables a rational method for choosing an ideal dispensation sequence based on the needs of a particular molecular laboratory. In our practice setting, the need for detecting all known *BRAF* mutations leads to the choice of the homebrew assay.

In summary, the virtual pyrogram is a useful tool for confirming hypothetical solutions to pyrosequencing results. Sequencing regions, such as *BRAF* codons 596 to 605, can produce pyrograms in which the starting point for iterative hypothesis testing is difficult to appreciate. Therefore, the lookup table of peak changes comprises a helpful adjunct to hypothesis testing. Because of the possibility of degeneracies, lookup table solutions of complex pyrograms should be confirmed with a virtual pyrogram.

Supplementary Material

Refer to Web version on PubMed Central for supplementary material.

Acknowledgments

This study was funded by grant P30 CA006973 from the National Institutes of Health, Bethesda, MD, and a Johns Hopkins Department of Pathology Young Investigator Award.

References

1. Davies H, Bignell GR, Cox C, et al. Mutations of the *BRAF* gene in human cancer. *Nature*. 2002; 417:949–954.
2. Cohen Y, Xing M, Mambo E, et al. *BRAF* mutation in papillary thyroid carcinoma. *J Natl Cancer Inst*. 2003; 95:625–627.
3. Tiacchi E, Trifonov V, Schiavoni G, et al. *BRAF* mutations in hairy-cell leukemia. *N Engl J Med*. 2011; 364:2305–2315. [PubMed: 21663470]
4. Singer G, Oldt R, Cohen Y, et al. Mutations in *BRAF* and *KRAS* characterize the development of low-grade ovarian serous carcinoma. *J Natl Cancer Inst*. 2003; 95:484–486. [PubMed: 12644542]
5. Yuen ST, Davies H, Chan TL, et al. Similarity of the phenotypic patterns associated with *BRAF* and *KRAS* mutations in colorectal neoplasia. *Cancer Res*. 2002; 62:6451–6455. [PubMed: 12438234]
6. Nikiforov YE, Ohori NP, Hodak SP, et al. Impact of mutational testing on the diagnosis and management of patients with cytologically indeterminate thyroid nodules: a prospective analysis of 1056 FNA samples. *J Clin Endocrinol Metab*. 2011; 96:3390–3397. [PubMed: 21880806]
7. Nikiforov YE, Steward DL, Robinson-Smith TM, et al. Molecular testing for mutations in improving the fine-needle aspiration diagnosis of thyroid nodules. *J Clin Endocrinol Metab*. 2009; 94:2092–2098. [PubMed: 19318445]

8. Lupi C, Giannini R, Ugolini C, et al. Association of BRAF V600E mutation with poor clinicopathological outcomes in 500 consecutive cases of papillary thyroid carcinoma. *J Clin Endocrinol Metab.* 2007; 92:4085–4090. [PubMed: 17785355]
9. Xing M, Westra WH, Tufano RP, et al. BRAF mutation predicts a poorer clinical prognosis for papillary thyroid cancer. *J Clin Endocrinol Metab.* 2005; 90:6373–6379. [PubMed: 16174717]
10. Di Nicolantonio F, Martini M, Molinari F, et al. Wild-type *BRAF* is required for response to panitumumab or cetuximab in metastatic colorectal cancer. *J Clin Oncol.* 2008; 26:5705–5712. [PubMed: 19001320]
11. Long GV, Menzies AM, Nagrial AM, et al. Prognostic and clinicopathologic associations of oncogenic *BRAF* in metastatic melanoma. *J Clin Oncol.* 2011; 29:1239–1246. [PubMed: 21343559]
12. Amanuel B, Grieu F, Kular J, et al. Incidence of BRAF p.Val600Glu and p.Val600Lys mutations in a consecutive series of 183 metastatic melanoma patients from a high incidence region. *Pathology.* 2012; 44:357–359. [PubMed: 22614711]
13. Menzies AM, Haydu LE, Visintin L, et al. Distinguishing clinicopathologic features of patients with V600E and V600K *BRAF*-mutant metastatic melanoma. *Clin Cancer Res.* 2012; 18:3242–3249. [PubMed: 22535154]
14. Tan YH, Liu Y, Eu KW, et al. Detection of *BRAF* V600E mutation by pyrosequencing. *Pathology.* 2008; 40:295–298.
15. Ogino S, Kawasaki T, Brahmandam M, et al. Sensitive sequencing method for *KRAS* mutation detection by pyrosequencing. *J Mol Diagn.* 2005; 7:413–421. [PubMed: 16049314]
16. Spittle C, Ward MR, Nathanson KL, et al. Application of a *BRAF* pyrosequencing assay for mutation detection and copy number analysis in malignant melanoma. *J Mol Diagn.* 2007; 9:464–471. [PubMed: 17690212]
17. Tsiatis AC, Norris-Kirby A, Rich RG, et al. Comparison of Sanger sequencing, pyrosequencing, and melting curve analysis for the detection of *KRAS* mutations. *J Mol Diagn.* 2010; 12:425–432. [PubMed: 20431034]
18. Chen G, Olson MT, O'Neill A, et al. A virtual pyrogram generator to resolve complex pyrosequencing results. *J Mol Diagn.* 2012; 14:149–159. [PubMed: 22316529]
19. Santarpia L, Sherman SI, Marabotti A, et al. Detection and molecular characterization of a novel *BRAF* activated domain mutation in follicular variant of papillary thyroid carcinoma. *Hum Pathol.* 2009; 40:827–833. [PubMed: 19200582]
20. Moretti S, Macchiarulo A, De Falco V, et al. Biochemical and molecular characterization of the novel *BRAF*^{V599Ins} mutation detected in a classic papillary thyroid carcinoma. *Oncogene.* 2006; 25:4235–4240. [PubMed: 16501605]
21. Willmore-Payne C, Holden JA, Tripp S, et al. Human malignant melanoma: detection of BRAF- and c-kit- activating mutations by high-resolution amplicon melting analysis. *Hum Pathol.* 2005; 36:486–493. [PubMed: 15948115]
22. Houben R, Becker JC, Kappel A, et al. Constitutive activation of the Ras-Raf signaling pathway in metastatic melanoma is associated with poor prognosis. *J Carcinogenesis.* 2004; 3:6.
23. Jones DTW, Kocalkowski S, Liu L, et al. Oncogenic *RAF1* rearrangement and a novel *BRAF* mutation as alternatives to *KIAA1549: BRAF* fusion in activating the MAPK pathway in pilocytic astrocytoma. *Oncogene.* 2009; 28:2119–2123. [PubMed: 19363522]
24. Wan PTC, Garnett MJ, Roe SM, et al. Mechanism of activation of the RAF-ERK signaling pathway by oncogenic mutations of B-RAF. *Cell.* 2004; 116:855–867. [PubMed: 15035987]
25. Fransen K. Mutation analysis of the *BRAF*, *ARAF* and *RAF-1* genes in human colorectal adenocarcinomas. *Carcinogenesis.* 2003; 25:527–533. [PubMed: 14688025]
26. Olson MT, Yergey AL. Calculation of the isotope cluster for polypeptides by probability grouping. *J Am Soc Mass Spectrom.* 2009; 20:295–302. [PubMed: 19026561]
27. Olson MT, Epstein JA, Yergey AL. De novo peptide sequencing using exhaustive enumeration of peptide composition. *J Am Soc Mass Spectrom.* 2006; 17:1041–1049. [PubMed: 16735127]
28. Stein SE. Estimating the probabilities of correct identification from mass spectral library searches. *J Am Soc Mass Spectrom.* 1994; 5:316–326. [PubMed: 24222569]

29. Olson MT, Blank PS, Sackett DL, et al. Evaluating reproducibility and similarity of mass and intensity data in complex spectra: applications to tubulin. *J Am Soc Mass Spectrom.* 2008; 19:367–374. [PubMed: 18207417]
30. Olson MT, Epstein JA, Sackett DL, et al. Production of reliable MALDI spectra with quality threshold clustering of replicates. *J Am Soc Mass Spectrom.* 2011; 22:969–975. [PubMed: 21953038]
31. Farach-Colton M, Ferragina P, Muthukrishnan S. On the sorting-complexity of suffix tree construction. *J ACM.* 2000; 47:987–1011.

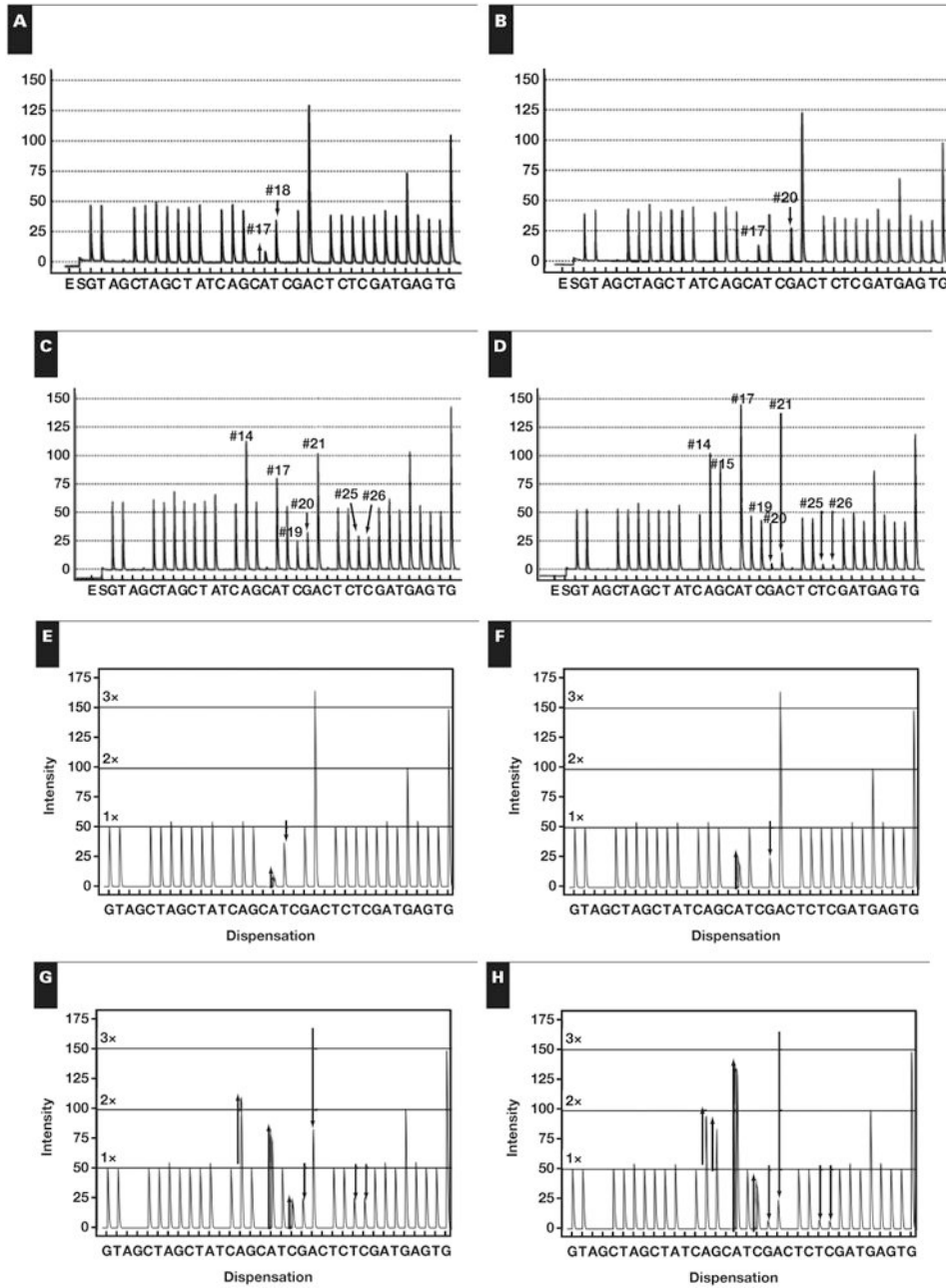


Figure 1. Nondegenerate clinical pyrograms and their confirmatory virtual pyrograms using the homebrew dispensation sequence. Shown are clinical pyrograms for **A**, V600E (c.1799T>A) and **B**, V600D (c.1799_1800delTGinsAT). Shown are pyrograms for **C**, V600K (c.1798_1799delGTinsAA) and **D**, V600R (c.1798_1799delGTinsAG). Figures **E-H** are the virtual pyrograms for these four mutations.

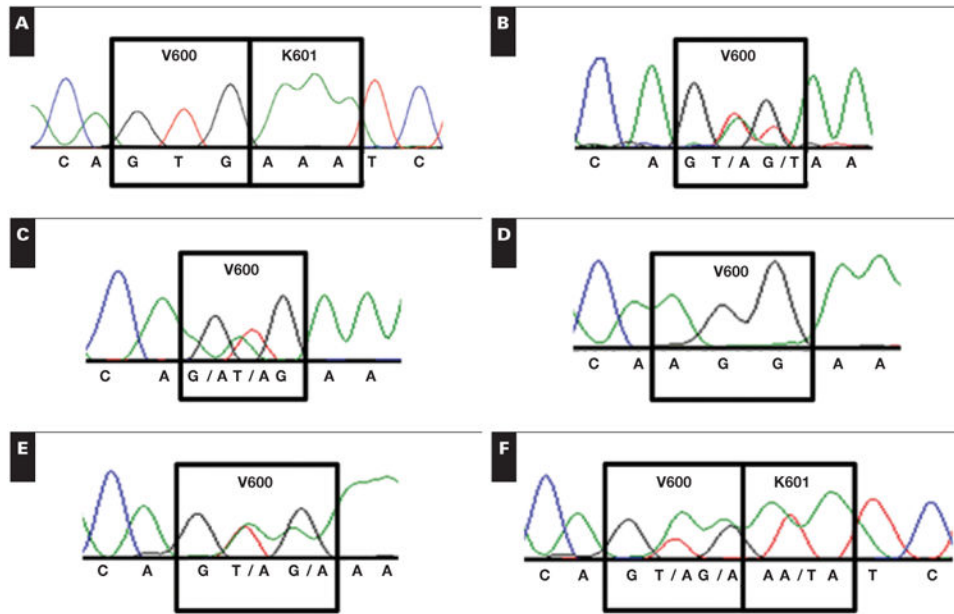


Figure 2.

Sanger confirmation for **A**, wild *BRAF* Sanger trace; **B**, V600D (c.1798_1800delGTGinsGAT); **C**, V600K (c.1798_1799delGTinsAA); **D**, V600_K601delinsEI (c.1799_1802delTGAAinsAAAT); **E**, homozygous V600R (c.1798_1799delGTinsAG); and **F**, V600E (c.1799_1800delTGinsAA).

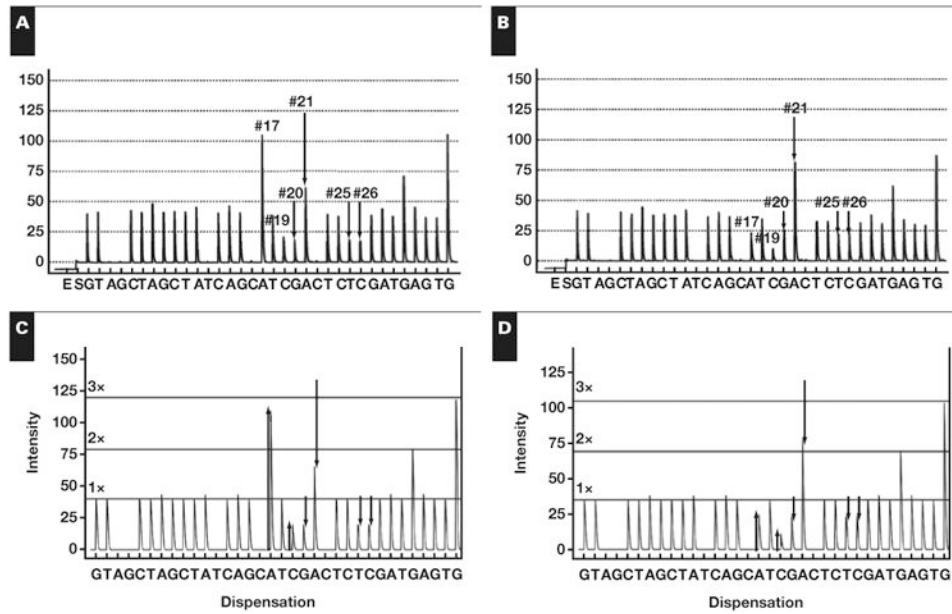


Figure 3. Two degenerate pyrograms. **A**, V600E (c.1799_1800delTGinsAA) and **B**, V600_K601delinsE (c.1799_1801delTGA). These are unambiguously resolved by the ratio of first and second changed peaks as shown in corresponding virtual pyrograms **C** and **D**.

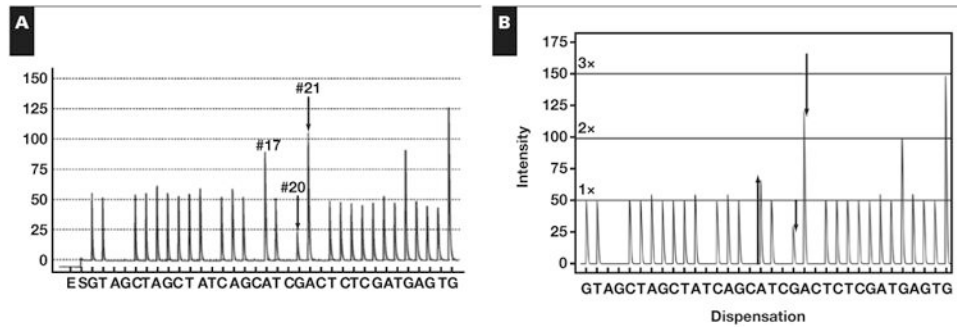


Figure 4. Hypothesis testing for a new mutation. **A**, Clinical pyrogram. **B**, The virtual pyrogram showing a new mutation, V600_K601delinsEI (c.1799_1802delTGAAinsAAAT).

Table 1

Expected Peak Changes for Pyrograms of *BRAF* Mutations

Mutation ^a	Homebrew Dispensation	Kit Dispensation	No. of Mutations	Activating ^b	Supplemental Figure ^c
L597L (c.1791A>G)	7,8 ^d	Not detected	3	No	1A
A598T (c.1792G>A)	7,8 ^d	Not detected	1	No	1B
A598V (c.1793C>T)	9,10	11,12 ^e	4	Yes ¹⁹	1C
A598_T599insV (c.1794_1795insGTT)	11,13,14,18,20,21,22,23, 24, 25,26,27,29,30,31,32,34	11,12 ^e	6	Yes ²⁰	1D
V600M (c.1798G>A)	14,15	6,7,8	20	No	2A
V600R (c.1798_1799delGTinsAG)	14,15,17,19,20,21,25,26	2,4,5,7,8 ^e	33	Yes ^{21,22}	2B
T599_V600insT (c.1796_1797insTAC)	14,15,20,21,22,23,24,25, 26, 27,29,30,31,32,34	4,5,7,8 ^e	3	Yes ²³	1E
V600R (c.1797_1799delAGTinsGAG)	14,17,18,20	2,4,5,8	1	Probably ²²	2C
V600K (c.1798_1799delGTinsAA)	14,17,19,20,21,25,26	4,5,7,8 ^e	183	Yes ^{21,22}	2D
V600G (c.1799T>G)	15,17,19,20,21,25,26	2,4,5,7,8 ^e	11	No	2E
V600E (c.1799T>A)	17,18	4,5	14,200	Yes ¹	2F
V600_K601delinsE (c.1799_1801delITGA)	17,19,20,21,25,26 ^d	Not sequenced	12	Yes ²²	2G
V600E (c.1799_1800delTGinsAA)	17,19,20,21,25,26 ^d	1,4,5,7,8	29	Probably ¹	2H
V600D (c.1799_1800delTGinsAT)	17,20	2,6	14	Yes ¹	2I
V600V (c.1800G>A)	20,21 ^d	1,2	1	No	2J
K601E (c.1801A>G)	20,21 ^d	Not sequenced	38	Yes ²⁴	3A
K601N (c.1803A>C)	21,22	Not sequenced	2	Yes ²⁵	3B
K601K (c.1803A>G)	21,23,24,25,26,28,30,31,32,33,34	Not sequenced	1	No	3C
K601N (c.1803A>T)	21,23	Not sequenced	6	No	3D
K601I (c.1802A>T)	21,24,25,26,27,30,31,32,33,34	Not sequenced	1	No	3E
V600_S605delinsEK (c.1799_1815delinsAAAAG)	17,18,20,21,23,24,25,26,27,28,29,30,31,32,33,34	Not sequenced	1	No	4F
V600_S605delinsD (c.1799_1814delinsA)	17,18,20,21,23,24,25,26,27,28, 29,30,31,32,33,34	Not sequenced	1	No	4C

^a Codons 595 to 605 only.^b Measured by ERK phosphorylation.^c Refers to comprehensive figures (examples of many of these can be found elsewhere in the article).

^pDegenerate peaks when using the homebrew dispensation.
^pDegenerate peaks when using the kit-based dispensation.

Author Manuscript

Author Manuscript

Author Manuscript

Author Manuscript